Yaseen A. Al-Soud*, Sondos O. Al-Sawakhnah, Raed A. Al-Qawasmeh, Najim A. Al-Masoudi*, Ala'a H. Al-Ahmad, Lamiaa Al-Maliki, Lasse van Geelen, Rainer Kalscheuer, Bahjat A. Saeed, Amneh Shtaiwi and Holger Stark

Novel 4-nitroimidazole analogues: synthesis, *in vitro* biological evaluation, *in silico* studies, and molecular dynamics simulation

https://doi.org/10.1515/znc-2023-0146
Received November 2, 2023; accepted March 20, 2024;
published online April 8, 2024

Abstract: A new series of 4-nitroimidazole bearing aryl piperazines **7**–**16**, tetrazole **17** and 1,3,4-thiadiazole **18** derivatives was synthesized. All derivatives were screened for their anticancer activity against eight diverse human cancer cell lines (Capan-1, HCT-116, LN229, NCI–H460, DND-41, HL-60, K562, and Z138). Compound **17** proved the most potent compound of the series inhibiting proliferation of most of the selected human cancer cell lines with IC_{50} values in the low micromolar range. In addition, compound **11** exhibited IC_{50} values ranging 8.60–64.0 μM against a selection of cancer cell lines. These findings suggest that derivative **17** can potentially be a new lead compound for further development of novel antiproliferative agents. Additionally, **17**–**18** were assessed for their antibacterial and antituberculosis activity. Derivatives **17** and **18** were the most potent compounds of this series against both *Staphylococcus aureus* strain Wichita and a methicillin resistant strain of *S. aureus* (MRSA), as well as against *Mycobacterium tuberculosis* strain mc^26230. The antiviral activity of **7**–**18** was also evaluated against diverse viruses, but no activity was detected. The docking study of compound **17** with putative protein targets in acute myeloid leukemia had been studied. Furthermore, the molecular dynamics simulation of **17** and **18** had been investigated.

Keywords: biological activity; cytotoxicity; docking study; 4-nitroimidazoles; molecular dynamics simulation

1 Introduction

Several substituted imidazole derivatives are of considerable pharmacological significance, particularly as antibacterial agents [1, 2], potential radiosensitizers [3], and anticancer agents [4, 5]. Dacarbazine (DTIC) 5-(3,3-dimethyl-1-triazeno) imidazole-4-carboxamide (Figure 1, **1**) [6, 7] is an anticancer drug and used in the treatment of metastatic melanoma [8, 9] as well as a part of the ABVD chemotherapy regimen to treat Hodgkin's lymphoma [10, 11] and in the MAID regimen for sarcoma [12]. Misonidazole (1-methoxy-3-(4-nitroimidazol-1-yl) propan-2-ol) (Figure 1, **2**) [13] is another imidazole analogue, reported as radiosensitizer and antineoplastic agents and is used for the treatment of hypoxic tumors [3], while Brown and Hirst [14] were reported the effect of clinical levels of misonidazole on the response of tumor and normal tissues in the mouse to alkylating agents. Furthermore, temozolomide (Temodar®) is classified as an alkylating agent commonly used to treat certain types of brain tumors such as glioblastoma multiforme or anaplastic astrocytoma [15, 16]. Other imidazole derivatives, such as metronidazole (Flagyl) **3** [17, 18], have been considered as potent azole antimycotic drugs (antifungal) and/or used as antiprotozoal agents (especially for the treatment of *Trichomonas vaginalis*, *Entamoeba histolytica*, and

***Corresponding authors: Yaseen A. Al-Soud**, Department of Chemistry, College of Science, University of Al al-Bayt, Al-Mafraq, Jordan, E-mail: alsoud@aabu.edu.jo. https://orcid.org/0000-0003-3357-3801; and **Najim A. Al-Masoudi**, Department of Chemistry, College of Science, University of Basrah, Basrah, Iraq, E-mail: najim.al-masoudi@gmx.de, Web: www.al-masoudi.de. https://orcid.org/0000-0001-6811-191X
Present address: Konstanz 78464, Germany; Department of Chemistry, College of Science, University of Basrah, Basrah, Iraq
Sondos O. Al-Sawakhnah and Ala'a H. Al-Ahmad, Department of Chemistry, College of Science, University of Al al-Bayt, Al-Mafraq, Jordan
Raed A. Al-Qawasmeh, Department of Chemistry, Pure and Applied Chemistry Group, College of Science, University of Sharjah, Sharjah 27272, UAE
Lamiaa Al-Maliki, Department of Molecular and Medical Biotechnology, Al-Nahrain University, Baghdad, Iraq
Lasse van Geelen and Rainer Kalscheuer, Institute of Pharmaceutical Biology and Biotechnology, Heinrich – Heine – University Düsseldorf, Duesseldorf 40225, Germany
Bahjat A. Saeed, Department of Chemistry, College of Education for Pure Science, University of Basrah, Basrah, Iraq
Amneh Shtaiwi, Faculty of Pharmacy, Middle East University, Queen Alia Airport Street, 11610, Amman, Jordan
Holger Stark, Institute of Pharmaceutical and Medicinal Chemistry, Heinrich – Heine – University Düsseldorf, Universitaetsstr. 1, 40225 Duesseldorf, Germany

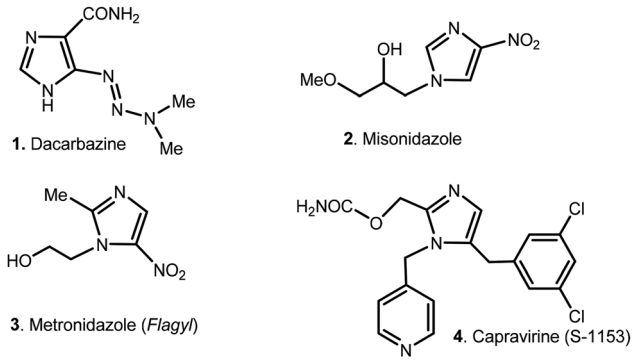

Figure 1: Selection of biologically active imidazole compounds.

Giardia lamblia). Capravirine (Figure 1, **4**) is an imidazole drug that potently inhibits HIV replication [19]. In addition, secnidazole (hydroxy-2-propyl)-l-methyl-2-nitro-5-imidazole) [20] and tinidazole (1-[2-(ethylsulfonyl)ethyl]-2-methyl-5-nitroimidazole) have been described for treatment of bacterial vaginosis [21].

Inspired by these reports on imidazole derivatives and in continuation of our previous work on imidazole analogues with antiviral and anticancer activity [22–31], we report here the synthesis of new nitroimidazole derivatives and the evaluation of their biological activities, such as, anticancer, antituberculosis, antibacterial and antiviral activities, as well as predictive molecular docking studies.

2 Results and discussion

2.1 Chemistry

1-Benzyl-5-bromo-2-methyl-4-nitroimidazole (**6**), prepared via two steps from the readily available 2-methyl-4-nitroimidazole (**5**) in our lab. [31], has been selected as a starting material for the synthesis of our new nitroimidazole derivatives *via* the nucleophilic displacement of the Br-substituent activated by an adjacent nitro group. Thus, treatment of **6** with various substituted piperazine analogues gave **7**–**16** in 81–70 % yield (Scheme 1).

The structure of **7**–**16** were confirmed on the basis of their ^{1}H, ^{13}C NMR, DEPT experiments since they showed similar patterns of aromatic protons and carbon atoms and are presented in Supplementary data, Figures S1–S30. In the ^{1}H NMR spectra of **7**–**16**, the phenyl and ethyl protons of the imidazole ring showed rather similar signaling patterns, whereas the singlets in the region δ_H = 5.16–5.01 ppm were attributed to the methylene of benzyl group. The eight methylene protons of the piperazine ring were appeared as broad singlet or multiplet in the region δ_H = 5.14–2.37 ppm. The other aliphatic and aromatic protons have been fully analyzed (*c.f.* Experimental section). In the ^{13}C NMR spectra of **7**–**16**, resonances in the region δ_C = 50.5–48.7 ppm were assigned to the methylene carbon atoms of benzyl group, whereas the signals at δ_C = 50.0–44.1 ppm were attributed to the piperazine carbons atoms. The downfield resonances in the region δ_C = 160.9–142.5 ppm were assigned to the pyridine carbon atoms of **7**–**9** and **12**–**14**. The resonances at δ_C = 154.8 and 142.0 ppm were attributed to the pyrazine carbon atoms, while the signals appeared at δ_C = 158.1 and 151.1 ppm were assigned to the quinoline carbon atoms. The other carbon atoms of aliphatic and aryl groups have been fully analyzed (*c.f.* Experimental section).

Analogously, replacement of the Br-substituent at C(5) of **6** by thiol residue of 1-phenyl-tetrazole-5-thiol (**A**) and 5-methyl-1,3,4-thiadiazole-2-thiol (**B**) under MWI at 90 °C proceeded smoothly to give **17** and **18** (69 and 70 % yield, respectively) (Scheme 2).

The structures of **17** and **18** were assigned on the basis of their ^{1}H, ^{13}C NMR spectra and DEPT experiments and are shown in Supplementary data, Figures S31–S36. The spectra showed similar patterns of aromatic protons and carbon atoms. In the ^{1}H NMR spectra of **17** and **18**, CH_2-Ph protons appeared as singlets at δ_H = 5.42 and 5.45 ppm, respectively. The aryl protons resonated as multiplets or doublets in the regions δ_H = 7.63–6.88 ppm, whereas the methyl protons appeared at δ_H = 2.73, 2.48, and 2.46 ppm. In the ^{13}C spectra of **17** and **18**, the down-field signals at δ_C = 148.1 and 167.0 ppm were assigned to C(5) of the tetrazole ring and carbon 2 of the 1,3,4-thiadiazole backbone, respectively. C-5 of the thiadiazole ring appeared at δ_C = 157.5 ppm, while the resonances at δ_C = 49.0 and 50.4 ppm was attributed to methylene carbon atoms of benzyl group, respectively.

2.2 Biological evaluation

In order to explore the biological activity of 1-(1-benzyl-2-methyl-4-nitro-1H-imidazole-5-yl)-4-(heteroaryl)piperazine **7**–**16** and 1-benzyl-2-methyl-5-(heteroarylthio)-4-nitro-1H-imidazole **17** and **18**, their *in vitro* anticancer, antituberculosis, antibacterial and antiviral activity were evaluated.

2.2.1 *In vitro* anticancer screening

The newly synthesized compounds **7**–**18** were screened for their anticancer activity on a diverse selection of human cancer cell lines: pancreatic adenocarcinoma (Capan)-1, colorectal carcinoma (HCT-116), glioblastoma (LN-229),

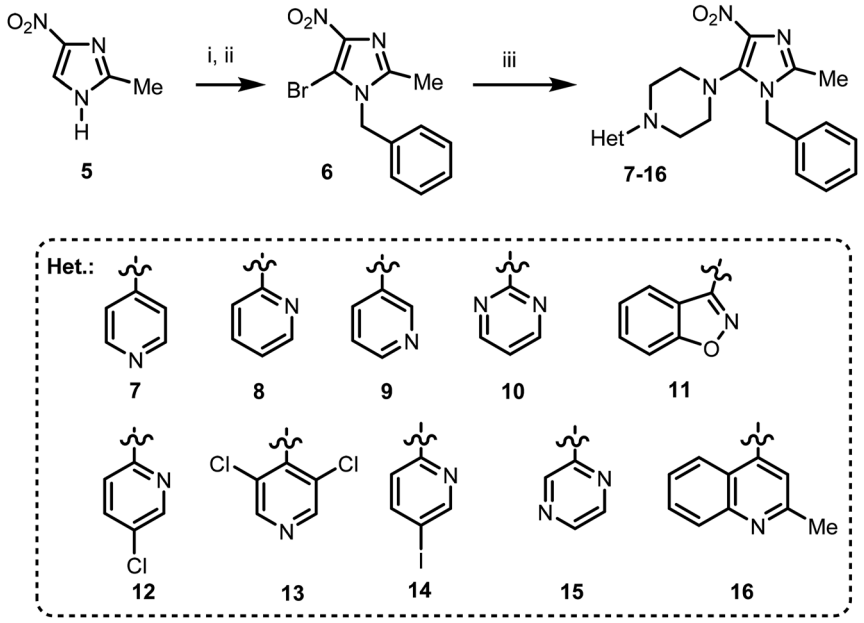

Scheme 1: *Reagents and conditions*: (i) DMF, $PhCH_2Cl$, 90 °C, 8 h. (ii) Br_2, reflux, 4 h; (iii) substituted hetaryl piperazine, *i*-propanol, microwave irradiation (MWI), 90 °C, 1.5 h.

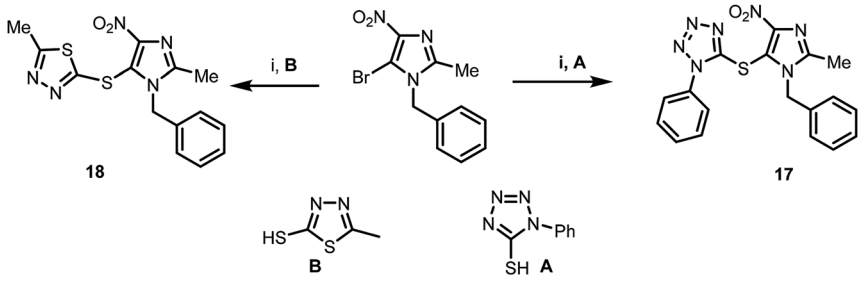

Scheme 2: *Reagents and conditions*: (i) 1-phenyl-1*H*-tetrazole-5-thiol (**A**) or 5-methyl-1,3,4-thiazdiazole-2-thiol (**B**), *i*-propanol, MWI, 90 °C, 1.5 h.

lung carcinoma (NCI–H460), acute lymphoblastic leukemia (DND-41), acute myeloid leukemia (HL-60), chronic myeloid leukemia (K-562), and non-Hodgkin lymphoma (Z-138) cancer cells (Table 1) using 3-(4,5-dimethylthiazol-2-yl)-5-(3-carboxymethoxyphenyl)-2-(4-sulfophenyl)-2*H*-tetrazolium (MTS) viability assay [32]. For comparison purposes, etoposide and nocodazole were used as reference drugs. Compound **17** proved the most active derivative of the series inhibiting proliferation of all the selected human cancer cell lines. It showed low micromolar IC_{50} values (ranging from 2.05 to 8.45 µM) against HL-60, Z-138, K-562, Capan-1, LN229, and HCT-116, while it exhibited a somewhat higher IC_{50} of 36.15 µM against the NCI–H460 cancer cell line. Compound **18** showed similar IC_{50} values (between 8.25 and 43.55 µM) against all cancer cell lines, while compound **11** exhibited selectivity toward the Capan-1, NCI–H460, HL-60, and Z-138 cell lines (IC_{50} values of 27.50, ≥64.0, 37.40, and 8.60 µM, respectively). In addition, compound **12** showed moderate activity against Capan-1, HL-60 and Z-138 (IC_{50} values of 88.1, 96.1 and 88.2 µM, respectively).

The SAR study revealed that the anticancer activity of compounds **7**–**18** was dependent on the nature of substituents in position-5 of the imidazole ring. Among all compounds tested, compound **17** with a phenyl-tetrazole substituent conjugated by a sulfur bridge on imidazole at position five demonstrated the most pronounced antitumoral activity. The results also state that heterocyclic groups conjugated to the piperazine ring at position four do not significantly impact the anticancer activity. In fact, these data encourage us to synthesize various substituted phenyl tetrazoles, which might enhance the antiproliferative effect on various cancer cell lines.

2.2.2 *In vitro* antiviral activity

Compounds **7**–**18** were also screened for their antiviral activity against several viruses HCoV-229E, -OC43, and -NL63 influenza, virus H1N1, H3N2 and B, RSV, HSV-1, yellow fever

Table 1: *In vitro* anticancer activity against a broad panel of cancer cell lines.

Comp.	IC_{50} (μM)							
	Cell lines							
	Capan-1	HCT-116	LN229	NCI–H460	DND-41	HL-60	K562	Z138
7	>100	>100	>100	>100	>100	>100	>100	>100
8	>100	>100	>100	>100	>100	>100	>100	>100
9	>100	>100	>100	>100	>100	>100	>100	>100
10	100	>100	>100	>100	>100	100	>100	>100
11	27.5	>100	>100	>64.0	>100	37.4	>100	8.6
12	88.1	>100	>100	>100	>100	96.1	>100	88.2
13	>100	>100	>100	>100	>100	>100	>100	>100
14	>100	>100	>100	>100	>100	>100	>100	>100
15	>100	>100	>100	>100	>100	>100	>100	>100
16	>100	>100	>100	>100	>100	>100	>100	>100
17	5.80	7.25	7.15	36.1	3.70	2.05	8.45	2.05
18	9.55	15.85	15.10	43.55	10.45	8.25	16.65	8.60
ETP	0.45	1.02	2.40	3.65	2.80	0.40	1.44	0.60
NDZ	0.09	1.45	2.40	3.65	0.45	0.10	0.07	0.30

ETP, etoposide; NDZ, nocodazole. Data represent mean of at least two independent experiments.

virus, Sindbis virus, Semliki Forest virus, and parainfluenza virus 3 as well as for their cytotoxicity on five virus host cell lines (HEL 299, Hep3B, MDCK, HEp-2, and VeroE6). The results can be found in Supplementary Table S2, with the cytotoxicity expressed as CC_{50} (50 % cytotoxic concentration) and antiviral activity as EC_{50} (50 % effective concentration), in which the data for remedesivir, ribavirin, zanamivir, rimantadine, acyclovir, and DS-10,000 are included for comparison purposes. None of these compounds showed any antiviral activity (EC_{50} > 50 μM) against the above panel of viruses at the highest concentration tested, with CC_{50} values of 50 μM.

2.2.3 In vitro antibacterial activity

The antibacterial activity of **7**–**18** was evaluated against nine different bacterial strains according to the CLSI standard protocol (CLSI) [33]. The Gram-positive bacterial strains comprised *Staphylococcus aureus* (ATCC-29,213 and MRSA strain ATCC-700,699) and *Enterococcus faecalis* (ATCC-29,212, vancomycin resistant strain ATCC-51,299, ATCC-35,667 and vancomycin and teicoplanin resistant strain ATCC-700,221), while the panel of Gram-negative bacteria included three different strains, namely *Acinetobacter baumannii* (drug resistant ATCC-BAA-1605), *Escherichia coli* (ATCC-25,922), and *Pseudomonas aeruginosa* (ATCC-27,853). The antibacterial potency was depicted as MIC (minimum inhibitory concentration) value. All compounds were inactive (MIC > 100 μM) against all bacteria strains except derivatives **17** and **18**, which exhibited MIC values of 3.12–6.25 and 50 μM against the Wichita strain (ATCC-29,213), respectively. Moreover, the same compounds showed comparable bactericidal activity with MIC values of 6.25 and 25 μM against the MRSA strain ATCC-700,699 (Table 2). The maximal tested concentration was 100 μM. Structure–activity relationship (SAR) reveals that the tetrazole and thiadiazole conjugated 5-nitroimidazole ring strongly enhance the antibacterial activity against *S. aureus*.

2.2.4 *In vitro* antituberculosis activity

Furthermore, compounds **7**–**18** were evaluated for *in vitro* antituberculosis activity (anti-TB) against *Mycobacterium tuberculosis* strain $mc^2$6230, using the resazurin dye reduction method to determine the actual minimum inhibitory concentration (MIC) [34]. Rifampicin was used as a reference drug. The MIC_{90} value was defined as the concentration inducing 90 % reduction in the fluorescence relative to control. All tested derivatives lacked activity against TB strain $mc^2$6230 (MIC > 100 μM), except for compounds **17** and **18** with MIC values of 100 and 25 μM, respectively (Figure 2).

Table 2: Antibacterial activity *in vitro* of the selected compounds **17** and **18** represented by MIC (μM).

	MIC_{50} (μM)								
Compd	**ATCC-29,213**	**ATCC-700,699**	**ATCC-29,212**	**ATCC-51,299**	**ATCC-35,667**	**ATCC-700,221**	**BAA-1605**	**ATCC-25,922**	**ATCC-27,853**
17	3.12–6.25	6.25	50	50	100	50	>100	>100	>100
18	50	25	100	100	100	100	>100	>100	>100

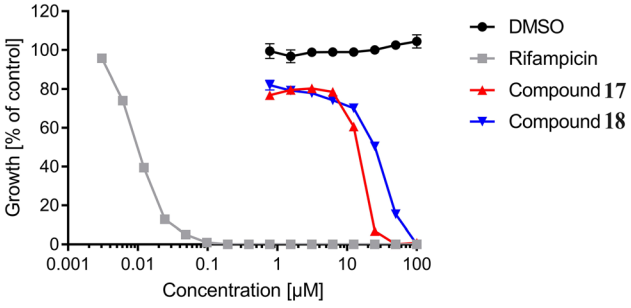

Figure 2: Dose–response curves of **17** and **18** against *M. tuberculosis* strain $mc^2$6230.

3 Molecular docking analysis

The goal of molecular docking calculations is to predict the most likely binding conformations and interactions between such a protein and a ligand [35].

In our search for a new anticancer lead derivative, we have selected compound **17** for molecular docking studies. Thus, molecular docking of **17** into the three-dimensional structure of acute myeloid leukemia (Fms-like tyrosine kinase 3 (FLT3) (PDB: 6JQR)), cell cycle related protein, CDK2/cyclin A2 (PDB: 7B7S), and protein kinase Akt1 PKB alpha (PDB: 4GV1) was performed using the MOE program. The prospective ligand was ranked according to the lowest energy of the best conformation. The calculated binding energy scores for compound **17** is −8.132 (RMSD = 1.390), −8.532 (RMSD = 1.562), and −7.830 (RMSD = 1.869) kcal mol^{-1}, respectively, indicating selectivity binding of this analogue to the active site of the protein receptor pockets (6JQR, 7B7S, and 4GV1, respectively).

Figure 3(A) showed docking of compound **17** oriented in an appropriate position for its binding with the protein receptors of acute myeloid leukemia (PDB: 6JQR) via two hydrogen bondings between N-3 and N-4 of the tetrazole moiety and Cys694. A π–H stacking interaction between the phenyl ring of benzyl group and Arg834. In addition, a π–H interaction between phenyl group of the tetrazole ring and Leu616 was observed. Nonbonded amino acid residues such as Asp829, Asn816, Arg815, Glus831, Cys828, Val624, Gly697, Lys644, and 644 of the receptor surrounded compound **17** were noticed.

Figure 3(B) demonstrated that the binding modes of **17** are settled down in the protein active site properly (PDB: 7B7S). It showed two π–H stacking interactions: one interaction between the aromatic ring of tetrazole residue of **17** and Asp145 was observed, while other interaction was indicated between tetrazole ring and Ala144. Additionally, it showed hydrogen bonding between N3 of the imidazole ring and Leu83. Furthermore, nonbonded amino acid residues such as His84, Phe80, Glu131, Val18, and Asn132 of the receptor surrounded the compound **17** were witnessed.

Figure 3(C) showed docking of **17** with protein kinase Akt1 PKB alpha receptor (PDB: 4GV1) via the two hydrogen bondings: bridged-sulfur atom and Asp292, and the other between N2 of tetrazole ring and Gly159. Besides these interactions, a bonding between H-imidazole ring and Met281 was observed. In addition, nonbonded amino acids such Lys158, Glys157, Val164, Glu278, and Lys179 of the receptor surrounded the compound **17** were observed. All the docked complex have shown expectable RMSD scores.

4 Molecular dynamics simulation

The stability of the top two tyrosine kinase-3 (FLT3) inhibitors, **17** and **18**, was selected for molecular dynamics simulation for the duration of 200 ns. MD simulation was performed to analyze the dynamic stability and development of intermolecular interactions of docked protein–ligand complexes. The resulting outcomes of 200 ns of each system were analyzed using root mean square deviation (RMSD), root mean square fluctuation (RMSF), hydrogen bond, and free energy analysis and are presented in Supplementary data (Sections S4.1–S4.4 and Figures S4–S7).

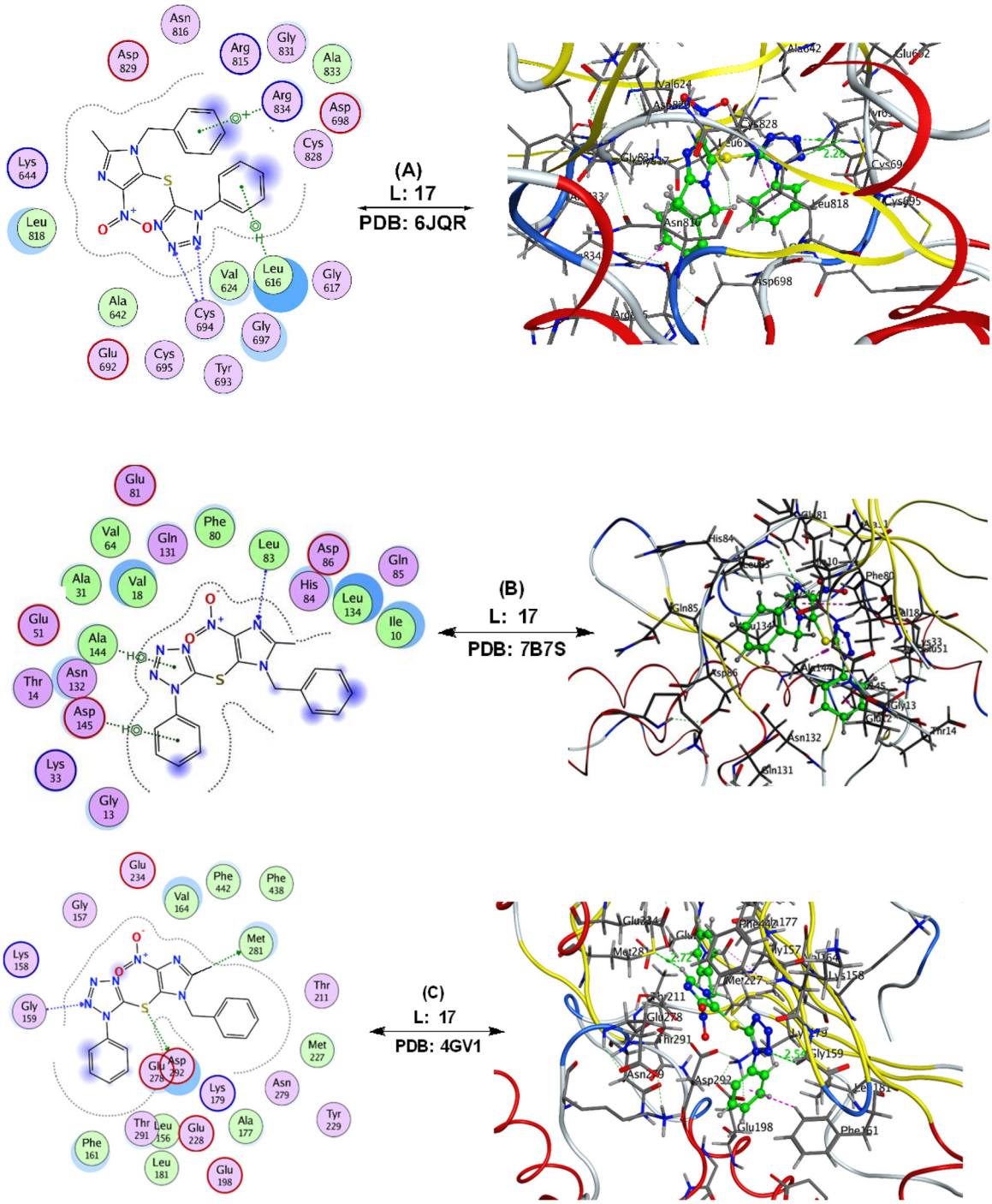

Figure 3: The interactions mode of compound **17** the protein with active site amino acids of the proteins (PDB ID's: 6JQR, 7B7S, and 4GV1, respectively).

5 Conclusions

In the present work, 4-nitroimidazole bearing substituted aryl piperazine 7–**16** have been synthesized from 1-benzyl-5-bromo-2-methyl-4-nitroimidazole (**6**) as a key intermediate via nucleophilic substitution of the active bromo residue. The key intermediate has been further modified by replacement of the bromo group of **6** by tetrazole and 1,3,4-thiadiazole derivatives to yield the new analogues **17** and **18**, respectively. All compounds were evaluated for their anticancer activity against eight human cancer cell lines (Capan-1, HCT-116, LN229, NCI–H460, DND-41, HL-60, K562, and Z138). The results were superior for derivatives **17** and **18**, with compound **17** being the most promising analogue of

the series showing low micromolar activity against most cancer cell lines. Furthermore, all compounds were screened for their antibacterial and antituberculosis activity. Here also, compounds **17** and **18** were found as the most potent derivatives of the series inhibiting the growth of *S. aureus* of strains ATCC-29,213 and ATCC-700,699, as well as *M. tuberculosis* strain mc^{2}6230. However, testing of **7**–**18** against several viruses revealed that these derivatives were devoid of antiviral activity against this panel of viruses. Furthermore, we investigated the stability and affinity of compounds **17** and **18** using molecular docking, MD simulation, and free energy calculations during the complexation with the protein of acute myeloid leukemia (tyrosine kinase-3). Molecular docking results showed interesting binding interaction of compound **17** with the active site of amino acid residues, especially, the Asp351 amino acid residue, which plays an important role in ligand-binding interactions. The flexibility and conformational change analysis based on the RMSD, RMSF, and hydrogen bond values revealed stable interactions with fewer conformational fluctuations for compound **17** ligand-binding interactions. In addition, the free energy calculations provided additional confirmation regarding the stability of complex **17**. The findings of this study offer valuable insights for the development of novel substituted-tetrazole 4-nitroimidazole analogues with potential as anticancer agents, as well as for future structural modifications.

6 Experimental

6.1 General

Chemicals sourced from Aldrich (Riedstraβe, Germany), Fluka (Buchs, Switzerland), and Scharlau are utilized without additional purification, unless specified otherwise. NMR spectra are obtained using either a Bruker Avance III-(500 MHz) or a Bruker DRX-300 spectrometer, with TMS serving as the internal standard. 1H NMR (500 MHz or 300 MHz) and ^{13}C NMR (125 MHz or 75 MHz) are recorded in deuterated chloroform ($CDCl_3$) or dimethylsulfoxide (DMSO-d_6). Chemical shifts are expressed in units of δ, reported in ppm, and J-coupling values for ^{1}H–^{1}H coupling constants are presented in Hertz (Hz). High-resolution mass spectra (HRMS) are obtained using the electrospray ion trap (ESI pos low mass) technique with collision-induced dissociation on a Bruker APEX-IV (7 T) instrument. Mass spectra (ESI) are measured on a TSQ Quantum instrument (Thermo Electron Corporation, Dreireich, Germany) equipped with an RP18 100-3 column (Macherey Nagel). Microwave-supported reactions were performed with microwave cavity or radio frequency (RF) (a special type of resonator) at 2.4 GHz, temperatures from 0 to 300 °C, in microwave reaction vials (2.5 mL) with Teflon septum and an aluminum crimp top. 1-Phenyl-1H-tetrazole-5-thiol (**A**) or 5-methyl-1,3,4-thiadiazole-2-thiol (**B**) have been purchased from Sigma-Aldrich company (Germany).

6.2 Synthesis

6.2.1 General procedure for the preparation of 1-(1-benzyl-2-methyl-4-nitro-1H-imidazol-5-yl)-4-(heteroaryl)piperazine (7–16): A suspension of **3** (0.5 mmol) and K_2CO_3 (0.5 mmol) in isopropanol (10 mL) was stirred at room temperature for 15 min and then heteroaryl piperazine (1.0 mmol) was added to the mixture. The reaction mixture was heated under microwave irradiation (MWI) at 90 °C for 1.5 h. Reaction was monitored by TLC, until TLC showed that the reactants were completely consumed. Evaporation of the solvent followed by extraction of the product with chloroform (20 × 3 mL). The organic phase was dried over anhydrous sodium sulfate, filtered, and evaporated to dryness, and then the residue was purified by TLC chromatography (eluent: ethyl acetate-hexane; 1:1) to give compounds 7–**16**.

6.2.1.1 Preparation of 5-((1-benzyl-2-methyl-4-nitro-1H-imidazol-5-yl) thio)-1-phenyl-1H-tetrazole (7): From 1-(pyridine-4-yl)piperazine (163 mg). Yield: 215 mg (78 %) as a yellow powder; m. p. 161–163 °C. – ^{1}H NMR (300 MHz, $CDCl_3$): δ = 8.10 (m, 2H, Hz, $H_{pyridine}$), 7.55–7.11 (m, 3H, ArH), 7.08–6.84 (m, 2H, ArH), 6.67–6.46 (m, 2H, $H_{pyridine}$), 5.08 (s, 2H, CH_2Ph), 4.20–2.60 (m, 8H, $H_{piperazine}$), 2.28 (s, 3H, CH_3). – ^{13}C NMR (75 MHz, $CDCl_3$): δ = 159.0 ($C_{pyridine}$), 147.6 ($C_{pyridine}$), 140.6 (C-2), 139.0 (C-4), 138.3 (C-5), 137.7 ($C_{pyridine}$), 134.6, 129.2, 128.2, 125.8 (Ph-C), 112.8 ($C_{pyridine}$), 108.2 ($C_{pyridine}$), 49.0 (CH_2Ph), 46.5, 45.75 ($C_{piperazine}$), 16.5 (CH_3). – MS ((+)-ESI): m/z = 378/379 $[M + H]^+$. – Anal. calcd. for $C_{20}H_{22}N_6O_2$: C 63.48; H 5.86; N 22.21; found: C 63.50; H 5.99, N 22.40 %.

6.2.1.2 Preparation of 1-(1-benzyl-2-methyl-4-nitro-1H-imidazol-5-yl)-4-(pyridin-2-yl)piperazine (8): From 1-(pyridine-2-yl)piperazine (163 mg). as a brown amorphous; Yield: 166 mg (70 %); m. p. 171–172 °C. – ^{1}H NMR (300 MHz, $CDCl_3$): δ = 8.08 (d, J = 5.5 Hz, 1H, $H_{pyridine}$), 7.65 (t, J = 8.0 Hz, 1H, $H_{pyridine}$), 7.38–7.24 (m, 3H, ArH), 7.05–6.70 (m, 4H, ArH + $H_{pyridine}$), 5.16 (s, 2H, CH_2Ph), 4.35–2.81 (m, 8H, $H_{piperazine}$), 2.30 (s, 3H, CH_3). – ^{13}C NMR (75 MHz, $CDCl_3$): δ = 155.2 ($C_{pyridine}$), 142.5 ($C_{pyridine}$), 141.1 ($C_{pyridine}$), 140.9 (C-2), 139.6 (C-4), 138.3 (C-5), 135.2, 129.30, 128.3, 125.9 (Ph-C), 113.3 ($C_{pyridine}$), 109.9 ($C_{pyridine}$), 48.7 (CH_2Ph), 46.7, 46.7 ($C_{piperazine}$), 14.1 (CH_3). – MS ((+)-ESI): m/z = 378/379 $[M + H]^+$. – Anal. calcd. for $C_{20}H_{22}N_6O_2$: C, 63.48; H, 5.86; N, 22.21; found: C, 63.61; H, 6.01; N 22.57.

6.2.2 Preparation of 1-(1-benzyl-2-methyl-4-nitro-1H-imidazol-5-yl)-4-(pyridin-3-yl)piperazine (9): From 1-(pyridine-3-yl)piperazine (163 mg). Yield: 169 mg (70 %), m. p. 166–168 °C. – ^{1}H NMR (300 MHz, $CDCl_3$): δ = 8.12 (d, J = 5.3 Hz, 2H, $H_{pyridine}$), 7.59–6.94 (m, 7H, ArH + $H_{pyridine}$), 5.07 (s, 2H, CH_2Ph), 3.70–2.88 (m, 8H, $H_{piperazine}$), 2.32 (s, 3H, CH_3). – ^{13}C NMR (75 MHz, $CDCl_3$): δ = 147.4 ($C_{pyridine}$), 140.7 (C-2), 139.7 (C-4), 138.4 (C-5), 137.5 ($C_{pyridine}$), 135.2 (PhC), 135.0 ($C_{pyridine}$), 129.3, 128.4, 125.8 (PhC), 124.9 ($C_{pyridine}$), 124.6 ($C_{pyridine}$), 48.8 (CH_2Ph), 48.6, 46.57 ($C_{piperazine}$), 14.1 (CH_3). – MS ((+)-ESI): m/z = 378/379 $[M+H]^+$. – Anal. calcd. for $C_{20}H_{22}N_6O_2$: C, 63.48; H, 5.86; N, 22.21; found: C, 63.59; H, 6.88; N, 22.52.

6.2.2.1 Preparation of 2-(4-(1-benzyl-2-methyl-4-nitro-1H-imidazol-5-yl) piperazin-1-yl)pyrimidine (10): From 4-(piperazin-1-yl)pyrimidine (164 mg). Yield: 340 mg (74 %) as orange powder; m. p. 180–182 °C. – ^{1}H NMR (300 MHz, $CDCl_3$): δ = 8.24 (d, 2H, J = 4.8 Hz, $H_{pyrimidine}$), 7.33–7.20 (m, 3H, ArH), 6.96 (d, 2H, J = 7.3 Hz, 2H, ArH), 6.47 (t, 1H, J = 4.8 Hz, $H_{pyrimidine}$), 5.10 (s, 2H, CH_2Ph), 3.06 (bs, 8H, $H_{piperazine}$), 2.29 (s, 3H, CH_3). – ^{13}C NMR (75 MHz, $CDCl_3$): δ = 160.9 ($C_{pyridine}$), 157. 7 ($C_{pyridine}$), 140.57 (C-2), 139.6 (C-4), 138.93 (C-5), 135.2, 129.3, 128.3, 125.9 (PhC), 110.6 ($C_{pyridine}$), 49.0

(CH_2Ph), 46.9, 44.1 ($C_{piperazine}$), 14.2 (CH_3). – MS ((+)-ESI): *m/z* = 379/380 $[M+H]^+$. – Anal. calcd. for $C_{19}H_{21}N_7O_2$: C, 60.15; H, 5.58; N, 25.84; found: C, 60.26; H, 5.69; N, 26.02.

6.2.2.2 Preparation of 3-(4-(1-benzyl-2-methyl-4-nitro-1H-imidazol-5-yl) piperazin-1-yl)-3a,7a-dihydrobenzo[d]isoxazole (11): From 3-(piperazin-1-yl)benzo[*d*]isoxazole (203 mg). Yield: 190 mg (81 %) as light yellow powder; m. p. 165–168 °C. – ^{1}H NMR (300 MHz, $CDCl_3$): δ = 7.65–7.08 (m, 8H, ArH + $H_{isoxazole}$), 7.04 (d, 1H, *J* = 7.0 Hz, ArH), 5.14–5.06 (m, 4H, $H_{piperazine}$), 5.04 (2H, CH_2Ph), 3.75–3.54 (m, 4H, $H_{piperazine}$), 2.19 (s, 3H, CH_3). – ^{13}C NMR (75 MHz, $CDCl_3$): δ = 164.0 ($CN_{oxazole}$), 161.4 ($CO_{oxazole}$), 140.7 (C-2), 139.7 (C-4, 138.6 (C-5), 135.2, 129.8, 129.4, 128.5, 125.9, 122.6, 122.0, 116.0, 110.6 (Ar–C), 48.9 (CH_2Ph), 48. 8, 46.6 ($C_{piperazine}$), 14.1 (CH_3). – MS ((+)-ESI): *m/z* = 418/419 $[M + H]^+$. – Anal. calcd. for $C_{22}H_{22}N_6O_3$: C, 63.15; H, 5.30; N, 20.0; found: C, 63.28; H, 5.49; N 20.22.

6.2.2.3 Preparation of 1-(1-benzyl-2-methyl-4-nitro-1H-imidazol-5-yl)-4-(5-chloropyridin-2-yl)piperazine (12): From 1-(5-chloropyridine-2-yl) piperazine (197 mg). Yield: 183 mg (73 %) as a light brown powder; m. p. 145–147 °C. – ^{1}H NMR (300 MHz, $CDCl_3$): δ = 8.10 (s, 1H, $H_{pyridine}$), 7.42–7.28 (m, 4H, ArH + $H_{pyridine}$), 7.04 (d, 2H, *J* = 7.3 Hz, ArH), 6.60 (d, 1H, *J* = 9.0 Hz, $H_{pyridine}$), 5.16 (s, 2H, CH_2Ph), 4.06–3.19 (m, 8H, $H_{piperazine}$), 2.37 (s, 3H, CH_3). – ^{13}C NMR (75 MHz, $CDCl_3$): δ = 157.5 ($CCl_{pyridine}$), 146.2 ($CN_{pyridine}$), 140.6 (C-2), 139.6 (C-4), 138.9 (C-5), 137.2 ($C_{pyridne}$), 135.2, 129.3, 128.3, 125.9, 120. 7 (PhC), 108.1 ($C_{pyridine}$), 48.9 (CH_2Ph), 46.5, 45.7 ($C_{piperazine}$), 14.1 (CH_3). – MS ((+)-ESI): *m/z* = 412/414 $[M+H]^+$. – Anal. calcd. for $C_{20}H_{21}ClN_6O_2$: C, 58.18; H, 5.13; N, 20.36; found: C, 58.33; H, 5.19; N, 20.51.

6.2.2.4 Preparation of 1-(1-benzyl-2-methyl-4-nitro-1H-imidazol-5-yl)-4-(3,5-dichloropyridin-2-yl) piperazine (13): From 1-(3,5-dichloropyridine-2-yl)piperazine (232 mg). Yield: 178 mg (75 %); m. p. 185–188 °C. – ^{1}H NMR (300 MHz, $CDCl_3$): δ = 8.1 9 (s, 1H, $H_{pyridine}$), 7.48–7.25 (m, 5H, ArH + $H_{pyridine}$), 7.03 (d, 1H, *J* = 7.3 Hz, ArH), 5.16 (s, 2H, CH_2Ph), 3.19–2.37 (m, 8H, $H_{piperazine}$), 2.37 (s, 3H, CH_3). – ^{13}C NMR (75 MHz, $CDCl_3$): δ = 151.1 ($CCl_{pyridine}$), 149.2 ($CN_{pyridine}$), 140.6 (C-2), 139.3 ($CH_{pyridine}$), 139.6 (C-4), 139.0 (C-5), 135.2, 129.3, 128.3, 126.0 (PhC), 114.1 ($C_{pyridine}$), 50.5 (CH_2Ph), 49.8, 46.5 ($C_{piperazine}$), 14.2 (CH_3). – MS ((+)-ESI): *m/z* = 446/448/450 $[M + H]^+$. – Anal. calcd. for $C_{20}H_{20}Cl_2N_6O_2$: C, 53.70; H, 4.51; N, 18.79; found: C, 53.91; H, 4.67; N, 18.93.

6.2.2.5 Preparation of 1-(1-benzyl-2-methyl-4-nitro-1H-imidazol-5-yl)-4-(5-iodopyridin-2-yl) piperazine (14): From 1-(iodopyridine-2-yl)piperazine (289 mg). Yield: 180 g (79 %) as a dark brown powder; m. p. 175–178 °C. – ^{1}H NMR (300 MHz, $CDCl_3$): δ = 8.23 (s, 1H, $H_{pyridine}$), 7.59 (d, 1H, *J* = 9.0, 2.3 Hz, $H_{pyridine}$), 7.44–7.22 (m, 3H, ArH), 6.95 (d, 2H, *J* = 7.2 Hz, ArH), 6.40 (d, *J* = 9.0 Hz, $H_{pyridine}$), 5.08 (s, 2H, CH_2Ph), 3.68–2.86 (m, 8H, $H_{piperazine}$), 2.29 (s, 3H, CH_3). – ^{13}C NMR (75 MHz, $CDCl_3$): δ = 157.5 (I-$C_{pyridine}$), 146.2 ($CN_{pyridine}$), 140.6 (C-2), 139.6 (C-4), 138.9 (C-5), 137.2, 135.2, 129.3, 128.3, 125.9, 120.7, 108.1 ($C_{arom.}$), 48.9 (CH_2Ph), 46.5, 45.8 ($C_{piperazine}$), 14.1 (CH_3). – MS ((+)-ESI): *m/z* = 442/443 $[M + H]^+$. – Anal. calcd. for $C_{25}H_{26}N_6O_2$: C, 67.86; H, 5.92; N, 18.99; found: C, 68.08; H, 6.14; N 19.24.

6.2.2.6 Preparation of 2-(4-(1-benzyl-2-methyl-4-nitro-1H-imidazol-5-yl) piperazin-1-yl)pyrazine (15): From 2-(piperazin-1-yl)pyrazine (164 mg). Yield: 176 mg, (76 %) as a yellow powder; m. p. 177–179 °C. – ^{1}H NMR (300 MHz, $CDCl_3$): δ = 8.00 (d, 2H, *J* = 9 Hz, $H_{pyrazine}$), 7.77 (s, 1H, $H_{pyrazine}$), 7.26 (m, 3H, ArH), 6.92 (d, *J* = 8.1 Hz, 2H, ArH), 5.06 (s, 2H, CH_2Ph), 3.30–3.09 (s, 8H, $H_{piperazine}$), 2.26 (s, 3H, CH_3). – ^{13}C NMR (75 MHz, $CDCl_3$): δ = 154.8 ($C_{pyrazine}$), 142.0 ($C_{pyrazine}$), 140.7 (C-2), 139.7 (C-4), 138.6 (C-5), 135.2, 132.7 ($C_{pyrazine}$), 130.6, 129.3, 128.4, 125.8 ($_{Carom.}$), 48.8 (CH_2Ph), 46.6, 44.9 ($C_{piperazine}$), 14.1 (CH_3). – MS ((+)-ESI): *m/z* = 379/380 $[M + H]^+$. – Anal. calcd. for $C_{19}H_{21}N_7O_2$: C, 60.15; H, 5.58; N, 25.84; found: C, 60.33; H, 5.76; N, 26.04.

6.2.2.7 Preparation of 4-(4-(1-benzyl-2-methyl-4-nitro-1H-imidazol-5-yl) piperazin-1-yl)-2-methylquinoline (16): From 2-methyl-4-(piperazin-1-yl) quinoline (227 mg). Yield: 186 mg (71 %); m. p. 180–182 °C. – ^{1}H NMR (300 MHz, $CDCl_3$): δ = 8.80 (d, 1H, *J* = 8.7 Hz, $H_{quinoline}$), 8.07–7.59 (m, 2H, $H_{quinoline}$), 7.56–7.29 (m, 4H, ArH), 7.19–7.01 (m, 2H, ArH + $H_{quinoline}$), 6.75 (s, 1H, $H_{quinoline}$), 5.01 (s, 2H, CH_2Ph), 3.98–3.48 (m, 8H, $H_{piperazine}$), 3.01 (s, 3H, CH_3), 2.29 (s, 3H, CH_3). 2.29 (2 × s, 6H, 2 × CH_3). – ^{13}C NMR (75 MHz, $CDCl_3$): δ = 158.1 (C=$N_{quinoline}$), 151.1 (C-$N_{quinoline}$), 147.2 (C-2), 140.6 (C-4), 138.5 (C-5), 135.3, 129.6, 129.3, 128.9, 128.3, 126.3, 126.1, 126.1, 123.7, 123.6 ($C_{arom.}$), 50.5 (CH_2Ph), 50.0, 46.6 ($C_{piperazine}$), 24.5 (quinoline-CH_3), 14.2 (imidazole-CH_3). – MS ((+)-ESI): *m/z* = 442/443 $[M + H]^+$. – Anal. calcd. for $C_{25}H_{26}N_6O_2$: C, 67.86; H, 5.92; N, 18.99; found: C, 68.08; H, 6.14; N 19.24.

6.2.3 General procedure for the preparation of 1-benzyl-2-methyl-5-(heteroarylthio)-4-nitro-1H-imidazoles (17 and 18): A suspension of **6** (0.5 mmol) and K_2CO_3 (0.5 mmol) in isopropanol (10 mL) was stirred at room temperature for 15 min followed by the addition of heteroaryl thiol (1.0 mmol). The reaction mixture was heated under microwave irradiation (MWI) at 90 °C for 1.5 h. The reaction was monitored by TLC, until TLC showed that the reactants were completely consumed. Evaporation of the solvent followed by extraction of the product with chloroform (3 × 20 mL). The organic phase was dried over anhydrous sodium sulfate, filtered, and evaporated to dryness, and then the residue was purified by TLC chromatography (eluent: ethyl acetate-hexane; 1:1) to give the desired products.

6.2.3.1 5-((1-Benzyl-2-methyl-4-nitro-1H-imidazol-5-yl)thio)-1-phenyl-1H-tetrazole (17): From 1-(phenyl-tetrazole-5-thiol (178 mg). Yield: 199 mg (69 %) as a dark brown amorphous; m. p. 196–198 °C. – ^{1}H NMR (300 MHz, $CDCl_3$): δ = 7.63 (s, 5H, ArH), 7.47–7.27 (m, 3H, ArH), 7.15–6.88 (m, 2H, ArH), 5.42 (s, 2H, CH_2Ph), 2.48 (s, 3H, CH_3). – ^{13}C NMR (75 MHz, $CDCl_3$): δ = 148.1 ($C_{tetrazole}$), 133.7 (C-2), 133.0, 131.0, 130.0, 129.4, 128.7, 126.1, 124.4, 113.7 ($_{Carom.}$), 49.0 (CH_2Ph), 14.5 (CH_3). – MS ((+)-ESI): *m/z* = 393/394 $[M + H]^+$. – Anal. calcd. for $C_{18}H_{15}N_7O_2S$: C, 54.95; H, 3.84; N, 24.92; found: C, 55.19; H, 3.97; N, 25.11.

6.2.3.2 2-((1-Benzyl-2-methyl-4-nitro-1H-imidazol-5-yl)thio)-5-methyl-1,3,4-thiadiazole (18): From 5-methyl-1,3,4-thiadiazole-2-thiol (132 mg). Yield: 180 mg (70 %); m. p. 188–190 °C. – ^{1}H NMR (300 MHz, $CDCl_3$): δ = 7.35 (m, 3H, ArH), 7.04 (d, 2H, *J* = 6.9 Hz, ArH), 5.45 (s, 2H, CH_2Ph), 2.73, 2.46 (2 × s, 6H, 2 × CH_3). – ^{13}C NMR (75 MHz, $CDCl_3$): δ = 167.0 ($C_{thiadiazole}$-2), 157.5 ($C_{thiadiazole}$-5), 145.3 ($C_{imidazole}$-NO_2), 135.6, 129.4, 124.0 ($C_{arom.}$), 50.4 (CH_2Ph), 15.8, 14.5 (2xCH_3). – MS ((+)-ESI): *m/z* = 347/348 $[M + H]^+$. – Anal. calcd. for $C_{14}H_{13}N_5O_2S_2$: C, 48.40; H, 3.77; N, 20.16 %; found: C, 48.61; H, 3.95; N, 20.37.

6.3 Biological activity

6.3.1 Anticancer activity *in vitro*

6.3.1.1 Cancer cell lines: The American Type Culture Collection (ATCC, Manassas, VA, USA) provided the human cancer cell lines used in this manuscript, including Capan-1, HCT-116, LN-229, NCI–H460, HL-60, K-562, H, and Z-138 cancer cells, while the Deutsche Sammlung von Mikroorganismen und Zellkulturen (DSMZ Leibniz-Institute, Germany)

provided the DND-41 cell line. Except for the media for other cell lines, which were bought from Sigma, culture media were purchased from Gibco Life Technologies, USA, and supplemented with 10 % fetal bovine serum (HyClone, GE Healthcare Life Sciences, USA).

6.3.1.2 Proliferation assays: In 384-well tissue culture plates (Greiner), adherent cell lines LN-229, HCT-116, NCI–H460, and Capan-1 cells were seeded at a density of 500–1500 cells per well. Cells were exposed to seven different concentrations of the test substances, ranging from 100 to 0.006 M, after an overnight incubation period. Suspension cell lines HL-60, K-562, Z-138, and DND-41 were seeded in 384-well culture plates with the test chemicals at the same concentration points at densities ranging from 2500 to 5500 cells per well. The CellTiter 96® AQueous One Solution Cell Proliferation Assay (MTS) reagent (Promega) was used to evaluate the cells after they had been exposed to the chemicals for 72 h in accordance with the manufacturer's instructions. Using a SpectraMax, the samples' absorbance was measured at 490 nm and the optical density (OD) values were employed to calculate the 50 % inhibitory concentration (IC_{50}). The compounds were tested in two independent experiments.

6.3.2 Bacterial strains and growth conditions: Nosocomial bacterial reference strains were grown in Mueller–Hinton broth (MHB, Difco) at 37 °C. These included the Gram-positive species *S. aureus* (methicillin-susceptible *S. aureus* (MSSA) strain ATCC 29,213 and methicillin-resistant and vancomycin-intermediate *S. aureus* (MRSA/VISA) strain ATCC 700,699), *E. faecalis* (sensitive strain ATCC 29,212 and gentamycin-resistant strain ATCC 51,299), and *Enterococcus faecium* (sensitive strain ATCC 35,667 and vancomycin-resistant strain ATCC 700,221) as well as the Gram-negative species *E. coli* strain ATCC 25,922 (sensitive strain), multidrug-resistant *A. baumannii* strain ATCC BAA 1605, and multidrug-resistant *P. aeruginosa* strain ATCC 27,853.

6.3.3 Determination of the minimal inhibitory concentration: The minimal inhibitory concentration (MIC) against the tested nosocomial bacteria was determined according to the CLSI standard protocol [33]. Briefly, bacterial cells were grown aerobically in MHB medium at 37 °C and 180 rpm. A preculture was grown until log phase ($OD_{600\ nm}$–0.5) and then seeded at 5×10^4 CFU/well in a total volume of 100 µL in 96 well round-bottom microtiter plates and incubated with serially diluted test substances at a concentration range of 100–0.78 µM. Microplates were statically incubated aerobically at 37 °C for 24 h. MICs were determined macroscopically by identifying the minimum concentration of the compounds that led to complete inhibition of visual growth of the bacteria.

6.3.4 Antituberculosis assay: The attenuated *M. tuberculosis* Δ*RD1* Δ*panCD* strain ($mc^2$6230) was grown in Middlebrook 7H9 medium (Difco) supplemented with 10 % ADS (5 % bovine serum albumin fraction V, 2 % glucose, and 0.085 % NaCl), 0.5 % glycerol, 0.05 % tyloxapol, and 100 µg/mL pantothenic acid and incubated at 37 °C. The MIC against *M. tuberculosis* strain $mc^2$6230 was determined via resazurin dye reduction assay [33]. Briefly, the $OD_{600\ nm}$ of a pregrown *M. tuberculosis* culture ($OD_{600\ nm}$ = 0.4–0.8) was measured, and the cell density was adjusted to an $OD_{600\ nm}$ of 0.006 (equivalent to 2×10^6 CFU/mL). About 50 microliters of this cell suspension were added to a sterile polystyrene 96-well U-bottom plate (Sarstedt, Germany) containing a 1:1 serial dilution of test compounds at final test concentrations ranging from 100 µM to 0.78 µM. The plates were statically incubated for 5 days at 37 °C, 5 % CO_2, and humified atmosphere. After the incubation time, 10 µL of a 100 µg/mL resazurin solution were added to each well, carefully resuspended and incubated for another 16 h at ambient temperature. The cells were fixed for 30 min by adding 100 µL of a 10 % formalin solution. The readout was performed using a microplate reader (Tecan, Switzerland) to quantify the fluorescence at 540 nm (excitation) and 590 nm (emission). The growth was calculated in relation to the growth control (DMSO, vehicle) and the positive control rifampicin. All experiments were conducted in triplicates.

6.3.5 In vitro antiviral activity *in vitro* host cell lines: Antiviral assays toward human coronavirus (HCoV-229E and -OC43), herpes simplex virus-1 (HSV-1 KOS), and parainfluenza virus type 3 in HEL 299 cell cultures, RSV in HEp-2 cell cultures, Sindbis virus and Semliki Forest virus in VeroE6, yellow fever virus and human coronavirus (HCoV-NL63) in Hep3B cell cultures and influenza A/H1N1 (A/Ned/378/05), influenza A/H3N2 (A/HK/7/87), and influenza B (B/Ned/537/05) in MDCK cell cultures were performed. Serial dilutions of the test compounds were added in lieu of the growth medium on the day of the infection. A viral input of 100 CCID50 (the virus dosage required to infect 50 % of the cell cultures) was then given to each well after the virus had been diluted. On each virus host cell line, mock-treated cultures receiving only the test chemicals were added in order to assess the cytotoxicity. The formazan-based colorimetric assay was used to determine the virus-induced cytopathogenic impact after 3–7 days of incubation. 3-(4,5-Dimethylthiazol-2-yl)-5-(3-carboxymethoxyphenyl)-2-(4-sulfophenyl)CellTiter 96 AQueous One Solution Cell Proliferation Assay (from Promega, Madison, WI) and the antiviral activity were expressed as the 50 % effective concentration (EC_{50}). This assay measures the viability of cells using the compound 2-H-tetrazolium (MTS). Parallel to this, the mock-infected cells were used to generate the 50 % cytotoxic concentration (CC_{50}). Every experiment was carried out twice. The activities were contrasted with the reference activity (rifampicin).

7 *In silico* studies

7.1 Molecular docking

Molecular docking was done by the software MOE (Molecular Operating Environment) version 15.10 [36]. The ligands were sketched by the MOE builder and their energies were minimized using the energy minimization algorithm implemented in MOE. After water molecules were removed from their structures, the receptors were subjected to correction and 3D protonation refinement. The final structures were energy minimized using the Amber10:ETH force field at 0.00001 RMS gradient. The resulting structures of the proteins were subjected to molecular docking docked with the ligands via the MOE software.

7.2 Molecular dynamics simulation and free energy calculations

The 200 ns MD simulations were done using the program GROMACS (v2023.1) [37], with the all-atom additive CHARMM36 force field [38]. The TIP3P water model was used throughout the study [39]. The topologies of molecules **17** and **18** were generated with the CGenFF server. The initial configuration of the protein–ligand was energy minimized as a first step using the steepest descent algorithm. The energy tolerance was lower than 1000.0 kJ mol^{-1}. In the next step, the system was equilibrated in the NVT ensemble at 300 K with Berednsen thermostat [40] for 20 ps with a coupling constant of τT = 0.1 ps. This step was followed by equilibrating the system in the NPT ensemble at constant temperature (T = 300 K) and constant pressure (p = 1.015 bar) for a further 200 ps using the Parrinello–Rahman barostat [41] with τP = 2.0 ps. In the final step, the system was subjected to the production molecular dynamics simulation using the Parrinello–Rahman barostat with coupling constants of τT = 0.1 and τP = 2.0 ps, respectively. Free energy calculations were performed using the molecular mechanics Poisson–Boltzmann surface area (MM-PBSA) method available in the GROMACS software package prepared using the g_mmpbsa tool. In this study, MD trajectories for 200 ns of the simulation were chosen as the equilibrium part of the trajectory for energy analysis [42].

Supplementary information

((4.1 Root mean squared deviation (RMSD) and Figure 4, 4.2 Root mean square fluctuation (RMSF) and Figure 5, 4.3 Hydrogen bonds analysis and Figure 6, 4.4 Free energy calculations and Figure 7)); ^{1}H, ^{13}C NMR and DEPT spectra of representative compounds 7 (Figures S1–S3), **8** (Figures S4–S6), **9** (Figures S7–S9), **10** (Figures S10–S12), **11** (Figures S13–S15), **12** (Figures S16–S18), **13** (Figures S19–S21), **14** (Figures S22–S24), **15** (Figures S25–S27), **16** (Figures S28–S30), **17** (Figures S31–S33), **18** (Figures S34–S36).

Acknowledgments: We acknowledge Leentje Persoons and Dirk Daelemans from the Laboratory of Virology and Chemotherapy, KU Leuven, Belgium for the antitumoral and antiviral testing of the compounds.
Research ethics: Not applicable.
Author contributions: All the authors have accepted responsibility for the entire content of the submitted manuscript and approved submission.
Competing interests: The authors declare no conflicts of interest regarding this article.
Research funding: This work was supported by the Ministry of Higher Education, Jordan (Grant No. Bas 1/1/2017) and partial support of DFG GRK2158.
Data availability: Not applicable.

References

1. Daraji DG, Rajani DP, Rajani SD, Pithawala EA, Jayanthi S, Patel HD. Structure based design, synthesis, and biological evaluation of imidazole derivatives targeting dihydropteroate synthase enzyme. Bioorg Med Chem Lett 2021;36:127819.
2. Periwal P, Verma V, Kumar D, Kumar A, Bhatia M, Thakur S, et al. Novel azole–sulfonamide conjugates as potential antimicrobial candidates: synthesis and biological assessment. Future Med Chem 2024;16: 157–71.
3. Gong L, Zhang Y, Liu C, Zhang M, Han S. Application of radiosensitizers in cancer radiotherapy. Int J Nanomed 2021;16:1083–02.
4. Ali I, Lone NL, Aboul-Enein HY. Imidazoles as potential anticancer agents. Med Chem Comm 2017;8:1742–73.
5. Sharma P, LaRosa C, Antwi J, Govindarajan R, Werbovetz KA. Imidazoles as potential anticancer Agents: an update on recent studies. Molecules 2021;26:4213–79.
6. Patel N, Neupane R, Balaji S, Tiwari AK, Ray SD. Dacarbazine. Encyclopedia of toxicology, 4th ed.; 2024, vol 3:457–63 pp.
7. Lewis BC, Mackenzie PI, Miners JO. Application of homology modeling to generate CYP1A1 mutants with enhanced activation of the cancer chemotherapeutic prodrug dacarbazine. Mol Pharmacol 2011;80: 879–88.
8. Liu Q, Xu N, Liu L, Li J, Zhang Y, Shen C, et al. Dacarbazine-loaded hollow mesoporous silica nanoparticles grafted with folic acid for enhancing antimetastatic melanoma response. ACS Appl Mater Interfaces 2017; 26:21673–87.
9. Ugurel S, Paschen A, Becker JC. Dacarbazine in melanoma: from a chemotherapeutic drug to an immunomodulating agent. J Invest Dermatol 2013;133:289–92.
10. Yasuda H, Komatsu N, Ando J, Ando M. Hodgkin Lymphoma on hemodialysis: a review of treatment and recommendations. Clin Lymphoma, Myeloma & Leukemia 2022;22:805–11.
11. Brusamolino E, Baio A, Orlandi E, Arcaini L, Passamonti F, Griva V, et al. Long-term events in adult patient with clinical stage IA-IIA nobulky Hodgkins' lymphoma treated with four cycles of doxorubicin, bleomycin, vinblastine, and dacarvazine and adjuvant radiotherapy: a single-institution 15 year follow-up. Clin Cancer Res 2006;12:6487–93.
12. Adkins KE, Solimando DA, Waddell JA. Doxorubicin and dacarbazine (AD) regimen for soft tissue sarcomas. Hosp Pharm 2015;50:194–8.
13. Meißner R, Feketeová L, Illenberger E, Denifl S. Reactions in radiosensitizer misonidazole induced by low energy (0–10 eV(electrons). Int J Mol Sci 2019;20:3496.
14. Brown JM, Hirst DG. Effect of clinical levels of misonidazole on the response of tumour and normal tissues in the mouse to alkylating agents. Br J Cancer 1982;45:700–8.
15. Lee SY. Temozolomide resistance in glioblastoma multiforme. Genes Dis 2016;3:198–210.

16. Strobel H, Baisch T, Fitzel R, Schilberg K, Siegelin MD, Karpel-Massler G, et al. Temozolomide and other alkylating agents in glioblastoma therapy. Biomedicines 2019;7:69–86.
17. Huang Y, Shen C, Shen Y, Cui H. Assessing the efficacy of clotrimazole and metronidazole combined treatment in vaginitis: a meta-analysis. Alternative Ther Health Med 2024;30:186–91.
18. Cerulos AH, Romero-Quezada LC, Ledezma JC, López Contreras L. Therapeutic uses of metronidazole and its side effects: an update. Eur Rev Med Pharmacol Sci 2019;23:397–401. Contreras
19. Fujiwara T, Sato A, el-Farrash M, Miki S, Abe K, Isaka Y, et al. S-1153 inhibits replication of known drug-resistant strains of human immunodeficiency virus type 1. Antimicrob Agents Chemother 1998;42: 1340–5.
20. Nyirjesy P, Schwebke JR. Secnidazole: next-generation antimicrobial agent for bacterial vaginosis treatment. Future Microbiol 2018;13: 507–24.
21. Armstrong NR, Wilson JD. Tinidazole in the treatment of bacterial vaginosis; 2009, vol 1:59–65 pp.
22. Al-Soud YA, Al-Sa'doni H, Amajaour HAS, Al-Masoudi NA. Nitroimidazoles, Part 3. Synthesis and *anti*-HIV activity of new *N*-alkyl-4-nitroimidazoles bearing benzothiazole and benzoxazole backbones. Z Naturforsch 2007;62b:523–8.
23. Al-Soud YA, Al-Masoudi NA, De Clercqc E, Panneccoque C. Nitroimidazole Part 4. Synthesis and anti-HIV activity of new 5-alkylsulfanyl and 5-(4-arylsulphonyl)piperazinyl-4-nitroimidazole derivatives. Heteroat Chem 2007;18:333–40.
24. Al-Soud YA, Al-Masoudi NA, Hassan HG, De Clercqc E, Panneccoque C. Nitroimidazole Part 5. Synthesis and anti-HIV evaluation of new 5-substituted piperazinyl-4-nitroimidazole derivatives. Acta Pharm 2007;57:379–93.
25. Al-Masoudi NA, Al-Soud YA, De Clercq E, Paneccoque C. Nitroimidazoles Part 6. Synthesis, structure and in vitro anti-HIV activity of new 5-substituted piperazinyl-4-nitroimidazole derivatives. Antivir Chem Chemother 2007;18:191–00.
26. Al-Masoudi NA, Pfleiderer W, Pannecouque C. Nitroimidazole Part 7. Synthesis and anti-HIV activity of new 4-nitroimidazole derivatives. Z Naturforsch 2012;67b:835–42.
27. Al-Soud YA, Al-Masoudi NA, Al-Suod HH, Panneccoque C. Nitroimidazole Part 8. New 4-nitroimidazole derivatives as anti-HIV agents. Z Naturforsch 2012;67b:925–38.
28. Al-Soud YA, Al-Ahmad AH, Abu-Qatouseh L, Shtaiwi A, Alhelal KAS, Al-Suod HH, et al. Nitroimidazoles Part 9. Synthesis, molecular docking, and anticancer evaluations of piperazine-tagged imidazole derivatives. Z Naturforsch 2021;76b:523–8.
29. Al-Soud YA, Alhelal KAS, Saeed BA, Abu-Qatouseh L, Al-Suod HH, Al-Ahmad AH, et al. Synthesis, anticancer activity and molecular docking studies of new 4-nitroimidazole derivatives. ARKIVOC 2021;8:296–09.
30. Rasras AJ, Al-Qawasmeh RA, El-Naggar M, Shehadi I, Elaasser MM, Al-Soud YA. Design, synthesis and antimicrobial assessments of aminoacetyllenic-piperazine nitroimidazole hybrid compounds. Z Naturforsch 2023;78c:113–21.
31. Saber SOW, Al-Qawasmeh RA, Abu-Qatouseh L, Shtaiwi A, Khanfar MA, Al-Soud YA. Novel hybrid motifs of 4-nitroimidazole-piperazinyl tagged 1,2,3-triazoles:Synthesis, crystal structure, anticancer evaluations, and molecular docking study. Heliyon 2023;9:e19327.
32. Wang Y, Nguyen DT, Yang G, Anesi J, Kelly J, Chai Z, et al. Modified MTS proliferation assay for suspended cells to avoid the interference by hydralazine and β-mercaptoethanol. Assay Drug Dev Technol 2021;19: 184–90.
33. CLSI. Methods for dilution antimicrobial susceptibility tests for bacteria that grow aerobically: approved standard, 3rd ed. Clinical and Laboratory Standards Institute; 2015.
34. Taneja NK, Tyagi JS. Resazurin reduction assays for screening of anti-tubercular compounds against dormant and actively growing Mycobacterium tuberculosis, Mycobacterium bovis BCG and Mycobacterium smegmatis. J Antimicrob Chemother 2007;60:288–93.
35. Yu Meng X-Y, Zhang H-X, Mezei M, Cui M. Molecular docking: a powerful approach for structure-based drug discovery. Curr Comput Aided Drug Des 2011;7:146–57.
36. Molecular Operating Environment (MOE). 02 Chemical computing group ULC, 1010 Sherbooke St. West, Suite #910. Montreal, QC, Canada; 2022. H3A 2R7, 2023.
37. Abraham MJ, Murtola T, Schulz R, Páll S, Smith JC, Hess H, et al. GROMACS: high performance molecular simulations through multi-level parallelism from laptops to supercomputers. SoftwareX 2015;1: 19–25.
38. Vanommeslaeghe K, Hatcher E, Acharya C, Kundu S, Zhong S, Shim J, et al. CHARMM general force field (CGenFF): a force field for drug-like molecules compatible with the CHARMM all-atom additive biological force fields. J Comput Chem 2010;31:671–90.
39. Price DJ, Brooks CL. A modified TIP3P water potential for Simulation with ewald summation. J Chem Phys 2004;121:10096–03.
40. Messias A, Santos DES, Pontes FJS, Lima FS, Soares TA. Out of sight, out of mind: the effect of the equilibration protocol on the structural ensembles of charged glycolipid bilayers. Molecules 2020;25:5120. (16 pages).
41. Parrinello M, Rahman A. Polymorphic transitions in single crystals: a new molecular dynamics method. J Chem Phys 1981;52:7182–90.
42. Kumari R, Kumar R, Lynn A. G_mmpbsa–a GROMACS tool for high-throughput MM PBSA calculations. J Chem Inf Model 2014;54:1951–62.

Supplementary Material: This article contains supplementary material (https://doi.org/10.1515/znc-2023-0146).